Distributed Control of Photovoltaic Units in unbalanced LV Distribution Networks to Prevent Overvoltages

Frédéric OLIVIER, Raphaël FONTENEAU, Sébastien MATHIEU, Damien ERNST
Department of Electrical Engineering and Computer Science, University of Liège, Belgium
{frederic.olivier, raphael.fonteneau, smathieu, dernst}@uliege.be

***Abstract*—As more and more photovoltaic units are being installed, some LV networks have already attained their maximum hosting capacity, i.e. the maximum amount of distributed energy resources that they can accommodate during regular operations without suffering problems, such as overvoltages. As an alternative to network reinforcement, active network management (ANM) can, to a certain extent, increase their hosting capacity by controlling the power flows. In the framework of ANM, a distributed control scheme was previously presented. It makes use of a distress signal sent by each participating unit, when its terminal voltage is higher than 1.1 p.u. All units then proceed to absorb the maximum reactive power available. If the problem is not resolved, the units proceed to active power curtailment. This paper extends this control scheme to the case of unbalanced three-phase four-wire distribution networks with single- and/or three-phase inverters. The control scheme works by first partitioning the inverters into four groups, three for the single-phase inverters (one for each phase), and one for the three-phase converters. Each group then independently applies a distributed algorithm similar to the one previously presented. Their performance are then compared to those of two reference schemes, an on-off algorithm that models the default behaviour of PV inverters when there is an overvoltage, and the other one based on an unbalanced OPF. Its resulting total curtailed energy always lies between the two, with the on-off algorithm presenting the poorest performance, and the proposed algorithm losing its edge when the network is strongly unbalanced.**

***Index Terms*—Low-voltage distribution network, photovoltaic, overvoltage, distributed control, unbalance, three-phase.**

I. INTRODUCTION

More and more customers are reporting to Distribution System Operators (DSOs) that their PhotoVoltaic (PV) units are disconnecting from the network. This phenomenon has several causes, among which are occurrences of overvoltages in the low-voltage (LV) distribution feeder they are connected to. Indeed, as more PVs are being installed, some LV networks have already attained their maximum hosting capacity, i.e. the maximum amount of distributed energy resources (DER) that they can accommodate during regular operations without causing problems, such as violations of operational constraints (overvoltages and congestions). Norms impose the disconnection of a PV when the ten-minute average voltage at its connection point is higher than 110% of the nominal voltage, or when the instantaneous voltage surpasses 115% of the nominal voltage (cf. EN 50160). Theses disconnections cause a loss in renewable energy production and, henceforth, a loss of earnings for the PV owners.

To solve this problem, there are two alternative possibilities: on the one hand, reinforce the network or, on the other hand, control the power flows inside it by performing active network management (ANM), the focus of this paper. In the framework of ANM, several schemes to control the power generated by DER have been proposed in the literature, whether centralised or distributed. Since [1] provides a detailed literature review of the algorithms to control the PV units' output, we limit ourselves to references presenting control algorithm specifically designed for three-phase unbalanced networks. Papers [2], [3] present a centralized controller based on a multi-objective optimal power flow (OPF) problem that can simultaneously improve voltage magnitude and balance profiles, while minimizing network losses and generation costs. Paper [4] considers the economic dispatch distributed generation units with a semidefinite relaxation of the OPF. Paper [5] proposes an energy storage system for mitigating voltage unbalance as well as improving the efficiency of the network, using a local controller targeting specified voltage values. In particular, paper [1] presents a distributed control scheme which makes use of a distress signal sent by each participating unit when its terminal voltage is higher than 1.1 p.u. When this happens, all units proceed to absorb the maximum reactive power available. If the problem is not resolved, the units proceed to active power curtailment. This ensures a fair and coordinated use of reactive and active power.

The goal of the control scheme is to increase the hosting capacity of the network by controlling the power flows inside it. Incidentally, it maximises the active power production, or minimize the active power curtailed, which means minimising the occurrence of overvoltages.

This paper extends the algorithm developed in [1] to the case of unbalanced three-phase four-wire distribution networks with single- and/or three-phase inverters. Its key principles are inherited from the original algorithm proposed in [1] and are reiterated as follows: (i) it first makes use of reactive power, (ii) it uses active power curtailment as a last resort, (iii) it only needs communication in the form of a distress signal sent throughout the feeder to pool available resources, and (iv) it does not require a detailed model of the network.

The proposed algorithm is explained, illustrated and com-

pared to two other algorithms: an on-off algorithm – that models the default behaviour of PV inverters when there is an overvoltage – and an unbalanced optimal power flow. Their performance is compared in different PV connection scenarios, using three metrics: curtailed energy, reactive power usage and ohmic losses in the network.

The paper is organized as follows: Section II presents the modelling of the distribution system and its component throughout the entire paper. Section III presents the extension of the distributed algorithm presented in [1], and Section IV details the different algorithms to which it will be compared. Sections V and VI explain the scenarios for the numerical simulations and include an analysis of the results. Finally, Section VII concludes.

II. Modelling

To simulate the behaviour of the distribution system, the time will be discretised into multiple time steps for which successive steady-state power flows will be solved. This is motivated by the low inertia of the few rotating machines in LV networks, as well as the fast response of PV inverters. The following section defines the different modelling choices, as well as the different notations used in this paper. Throughout this section, the subscript t will refer to the current time step of simulation.

A. Buses

A node (a.k.a. bus) represents a connection point in the distribution system, e.g. a junction or a supply point. The set of node indices is $\mathcal{N}$. Throughout the network, there are four conductors, one for each phase identified, independently of the nodes, by their index set $\mathcal{P} = \{c_a, c_b, c_c\}$. The neutral conductor is referred to by c_n. Let $\mathcal{C} = \mathcal{P} \cup \{c_n\}$. Furthermore, the connection point of two or more conductors at a node is called a terminal. Double indexing is used to identify terminals, the first index referring to the node and the second one to the conductor. Using that convention, each terminal has a complex voltage $V_t^{(n,c)}\ \forall n \in \mathcal{N}, c \in \mathcal{C}$. The reference for this voltage is the common ground of the electrical system.

For proper operations of the network, the magnitude of the phase-to-neutral voltage should always lie between a lower bound $V_{\min}$ and an upper bound $V_{\max}$.

$$V_{\min} \leq \left| V_t^{(n,p)} - V_t^{(n,c_n)} \right| \leq V_{\max},\ \forall n \in \mathcal{N}, p \in \mathcal{P}. \quad (1)$$

B. Electrical lines

Electrical lines are called branches whether overhead lines or underground cables, and are identified by their index set $\mathcal{B}$. They are defined by a square impedance matrix $Z^{(b)}\ \forall b \in \mathcal{B}$, whose size is equal to the number of conductors, and which represents the resistance of the lines and the self- and mutual reactance of the conductors [6], [7]. The shunt capacitances are neglected, a choice commonly made (see, e.g., [8], [9], [10]) given the small length of LV lines and their small charging currents. The topology of the network is defined by associating to each branch a sending node n_s and a receiving node n_r. The currents flowing in each conductor, $I_t^{(b,c)}\ \forall b \in \mathcal{B}, c \in \mathcal{C}$, are considered to be positive if they flow from the sending node to the receiving node.

The voltage drop along the line is calculated with (2).

$$V_t^{(n_s,c)} - V_t^{(n_r,c)} = \sum_{c' \in \mathcal{C}} Z^{(b)}(c,c') I_t^{(b,c')}\ \forall b \in \mathcal{B}, c \in \mathcal{C} \quad (2)$$

Finally, when currents flow in a branch b, they generate losses $L_t^{(b)}$ according to Ohm's law:

$$L_t^{(b)} = \sum_{c \in \mathcal{C}} \sum_{c' \in \mathcal{C}} Z^{(b)}(c,c') \left(I_t^{(b,c')} \right)^2\ \forall b \in \mathcal{B} \quad (3)$$

C. Loads and photovoltaic units

The photovoltaic units (resp. the loads), whose index set is $\mathcal{G}$ (resp. $\mathcal{L}$), are defined by their injection of active $P_t^{(i,p)}$ and reactive power $Q_t^{(i,p)}\ \forall p \in \mathcal{P}, i \in \mathcal{G}$ (resp. $\forall i \in \mathcal{L}$), and the node to which they are connected, identified thanks to the function $N(\cdot)$ that links the index of a PV or load to the index of the node to which it is connected. $P_t^{(i,p)}$ and $Q_t^{(i,p)}$ are considered positive when the power is injected into the network.

$P_t^{(i)}$ and $Q_t^{(i)}$ refer to the total active and reactive power injected by PV or load i. In the case of a three-phase PV unit i, $P_t^{(i,p)} = P_t^{(i)}/3$ and $Q_t^{(i,p)} = Q_t^{(i)}/3, \forall p \in \mathcal{P}$. In the case of a single-phase PV unit i connected to phase p', $P_t^{(i,p')} = P_t^{(i)}$ and $Q_t^{(i,p')} = Q_t^{(i)}$, and $P_t^{(i,p)} = 0$ and $Q_t^{(i,p)} = 0, \forall p \in \mathcal{P} \backslash p'$.

The currents $I_t^{(i,p)}$ injected by the PV or load i in the phase conductor p of node $N(i)$ are calculated according to (4).

$$I_t^{(i,p)} = \left(\frac{P_t^{(i,p)} + jQ_t^{(i,p)}}{V_t^{(N(i),p)} - V_t^{(N(i),c_n)}} \right)^* \ \forall i \in \mathcal{L} \cup \mathcal{G}, p \in \mathcal{P} \quad (4)$$

where $(\cdot)^*$ denotes the complex conjugate.

The current $I_t^{(i,c_n)}$ injected by the PV or load i in the neutral conductor c_n is equal to the sum of the phase currents, as in Equation (5).

$$I_t^{(i,c_n)} = -\sum_{p \in \mathcal{P}} I_t^{(i,p)}\ \forall i \in \mathcal{G} \cup \mathcal{L} \quad (5)$$

The next three subsections describe the constraints limiting the production of PV units.

1) Maximum power point: Maximum power point tracking (MPPT) algorithms are implemented to maximise the output of the PV unit based on their I-V curve. In practice, this maximum production is not a priori known, as it depends on solar irradiance and the temperature of panels. For the purpose of this study, it is assumed that this point is known and equal to $P_{MPP,t}^{(i)}\ \forall i \in \mathcal{G}$, and that it limits the active power production according to (6).

$$P_t^{(i)} \leq P_{MPP,t}^{(i)}\ \forall i \in \mathcal{G} \quad (6)$$

2) Capability curve: The active power and reactive power production of a PV unit are limited by the capability curve of their inverter, i.e. they are limited by the maximum apparent power $S^{(i)}_{\max}$, $\forall i \in \mathcal{G}$ (7) and the minimum power factor $PF_{\min} = \cos\varphi_{\min}$ (8).

$$|P^{(i)}_t + jQ^{(i)}_t| \leq S^{(i)}_{\max} \ \forall i \in \mathcal{G} \tag{7}$$

$$-\tan\varphi_{\min} P^{(i)}_t \leq Q^{(i)}_t \leq \tan\varphi_{\min} P^{(i)}_t \ \forall i \in \mathcal{G} \tag{8}$$

As in [1], the one used in this study is coming from the German and Italian standards VDE-AR-N 405 and CEI 0-2. Those standards impose that the inverters are sized so that they can produce and absorb reactive power at the minimum power factor when the active power production is maximal. Henceforth, condition (7) will always be considered satisfied. For convenience, the function $Q^{(i)}_{\max}(P^{(i)}_t)$ gives the maximum amount of reactive power that PV unit i can produce or absorb, given its current active power production $P^{(i)}_t$.

3) Set points: $P^{(i)}_{set,t}$ (resp. $Q^{(i)}_{set,t}$) is the set point for active (resp. reactive) power of PV unit i. They are values that the control schemes can modify and optimise. If $P^{(i)}_{set,t}$ and $Q^{(i)}_{set,t}$ satisfy conditions (6) and (8), $P^{(i)}_t = P^{(i)}_{set,t}$ and $Q^{(i)}_t = Q^{(i)}_{set,t}$. If they do not, then they take the maximum values satisfying (6) and (8).

D. Slack bus

The equivalent of the external network is modelled as a slack bus whose voltages vary during the day according to on-site phase-to-neutral voltage measurements V_{SL}. The phase-to-neutral voltage of the slack bus (n_{SL}) is given by (9).

$$V^{(n_{SL},p)}_t - V^{(n_{SL},c_n)}_t = V^{(p)}_{SL,t}, \ \forall p \in \mathcal{P} \tag{9}$$

E. Kirchhoff's Current Law

Letting $\mathcal{B}^{(n)}_{in}$ (resp. $\mathcal{B}^{(n)}_{out}$) be the subset of lines whose receiving end (resp. sending end) corresponds to bus n, and $\mathcal{G}^{(n)}$ (resp. $\mathcal{L}^{(n)}$) be the subset of PV units (resp. loads) connected to node n, equation (10) implements Kirchhoff's current law.

$\forall n \in \mathcal{N}$,

$$I^{(b_{in},c)}_t + I^{(g,c)}_t + I^{(l,c)}_t = I^{(b_{out},c)}_t \tag{10}$$
$$\forall b_{in} \in \mathcal{B}^{(n)}_{in}, b_{out} \in \mathcal{B}^{(n)}_{out}, g \in \mathcal{G}^{(n)}, l \in \mathcal{L}^{(n)}, c \in \mathcal{C}$$

III. Distributed control scheme

To create the distributed control scheme, the inverters are first partitioned into four groups. The first three gather the single-phase inverters according to the phase to which they are connected, and the last group is composed of the three-phase inverters. Each group acts independently of the other ones, according to a distributed control scheme which is the direct extension of the one proposed in [1]. Its seven modes of operation as well as its state transition diagram are described in Section III-B and III-C.

Thanks to a distress signal (further explained in Section III-A), each phase group will react only if it records a voltage problem on its phase, and the three-phase group will react to all voltage violations. Doing so ensures that the actions of single-phase inverters do not create or worsen overvoltage situations, or even generate undervoltages. This also prevents the curtailment of active power in a phase where there is no overvoltage.

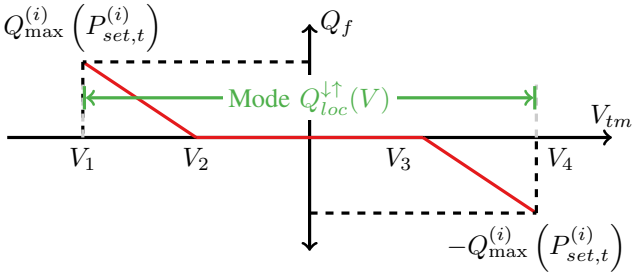

Fig. 1: $Q_f(V_{tm}, P_{set,t})$ function of PV unit i for Mode $Q^{\downarrow\uparrow}_{loc}(V)$, where V_{tm} is the voltage (resp. maximum voltage of the three-phase) at the connection point of the single-phase (resp. three-phase) PV unit. For $V_{tm} \geq V_4$ an emergency signal is issued, and the controller moves to Mode $Q^{\downarrow}$.

A. Distress signal

As a logical evolution from [1], where only one distress signal is sent when an overvoltage occurs, there are now three distress signals, one for each phase. They are repeatedly sent by the inverters recording an overvoltage in the phase to which they are connected. Three-phase inverters can thus send multiple distress signals if more than one phase suffer from an overvoltage.

B. Modes of operation

The controller is composed of seven modes of operations: one normal, two depleting, two waiting and two restoring ones. A detailed explanation of the modes is available in [1], and a short summary can be found in the next paragraphs. All modes are implemented as timers, i.e. once the inverter enters these modes, it will definitely exit them once their timer has elapsed. The normal mode of operation $Q^{\downarrow\uparrow}_{loc}(V)$ and the active power curtailment mode $P^{\downarrow}$ are two exceptions. Finally, all modes (except $Q^{\downarrow\uparrow}_{loc}(V)$) have a target for active and reactive power to reach at the end of the timer.

- Mode $Q^{\downarrow\uparrow}_{loc}(V)$ – normal mode of operation: The inverters maximise the active power with a Maximum Power Point Tracking (MPPT) algorithm. They absorb reactive power as a function of the local voltage (resp. maximal local voltage) for single-phase inverters (resp. for three-phase inverters). The function is illustrated in Figure 1.
- Mode $Q^{\downarrow}$ – depleting reactive power: the active power is at its maximum and the inverters gradually absorb reactive power until they reach the maximum at the end of a timer of t_{DQ} minutes. Once the time is up, the inverter moves to the next mode.
- Mode $P^{\downarrow}$ – curtailing active power: the reactive power absorption is maximal, and the active power production

is gradually lowered to reach zero at the end of a timer of t_{DP} minutes. When the timer ends, the inverter remains in this mode until there is no further distress signal.

- Mode $Q^{\rightarrow}$ – waiting to start increasing reactive power: once there is no further distress signal, the inverter enters a waiting mode of t_{reset} minutes to avoid rapid oscillations between depleting and restoring active and reactive power. In this mode, the active and reactive power set points remain constant.
- Mode $P^{\rightarrow}$ – waiting to start increasing active power: the active power set point remains constant for t_{reset} minutes and the reactive power absorption is maximal.
- Mode $P^{\uparrow}$ – restoring active power: the active power is gradually restored to its maximum. Since $P_{MPP,t}$ is not known a priori, the target for the active power is 110% of the installed capacity at the end of a timer of t_{RP} minutes. The reactive power absorption is maximal.
- Mode $Q^{\uparrow}$ – restoring reactive power: the inverters produce active power at its maximum. They gradually absorb less reactive power until they attain the value dictated by the function $Q_f(V)$ of Mode $Q_{loc}^{\downarrow\uparrow}(V)$ after t_{RQ} minutes.

C. State diagram

Figure 2 represents the state transition diagram of the controller. The red dotted lines are the emergency control transitions, i.e. when the PV unit receives a distress signal. The green dash-dotted lines represent the transition when there are no more distress signals. Finally, the blue dashed lines are the transition associated with the end of a timer. t_{DQ} (resp. t_{DP}) is the time needed in Mode $Q^{\downarrow}$ (resp. Mode $P^{\downarrow}$) to use all available reactive (resp. active) controls. t_{reset} is the elapsed time in Modes $Q^{\rightarrow}$ and $P^{\rightarrow}$ without an emergency signal for the controller to start restoring active/reactive power. t_{RP} (resp. t_{RQ}) is the time needed in Mode $P^{\uparrow}$ (resp. Mode $Q^{\uparrow}$) to restore active (resp. reactive) power to the set-point values of Mode $Q_{loc}^{\downarrow\uparrow}(V)$.

The four groups of inverters can be found in different locations of the state diagram, but all the inverters of the same group will be in the same mode. Indeed, they move from one mode to the other, thanks either to the timers or the presence or absence of a distress signal. Since three-phase PV units receive the distress signals from the three phases, they are more likely to stay in a depleting mode than a single-phase one.

D. Fairness

When curtailment of active power is inevitable, it is desirable for the control scheme to evenly distribute the burden among the PV units, a property known as 'fairness'.

However, the default behaviour of PV units that disconnect when there is an overvoltage is not fair, because this behaviour will likely curtail the PV units located further away from the beginning of the feeder, where the voltage sensitivity is higher, i.e. the ratio of voltage variations to the active and reactive power productions is larger.

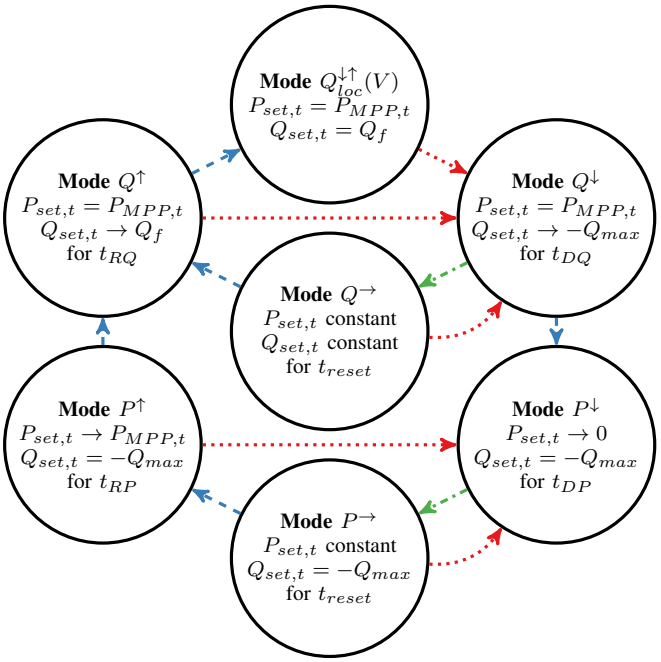

Fig. 2: State transition diagram of the distributed control scheme. The red dotted lines are the emergency control transitions, i.e. when the PV unit receives a distress signal. The green dash-dotted lines represent the transition when there are no more distress signals, and the blue dashed lines are the transition associated with the end of a timer. $P_{set,t}$ and $Q_{set,t}$ are the active and reactive power set-points of the controller. $P_{MPP,t}$ is the maximum available active power of the PV module and depends on the level of solar irradiation. Q_{max} is the maximum available reactive power; it varies according to the capability curve as a function of the active power output.

By contrast, the initial algorithm [1] was designed with fairness in mind as the curtailment was proportional to the installed capacity. The adaptation to three-phases is no longer fair in the same sense as it is now only fair group-wise.

E. Practical implementation

The controller can be implemented as a microcomputer. It can communicate with the inverter it controls thanks to RS-485 and the use of a proprietary communication protocol. It reads the voltage measurements in the appropriate registers of the micro-controller of the inverter, compute the active and reactive power set points according to the algorithm, and then write them in the appropriate registers.

Regarding the distress signal, if it is sent using Power Line Communication (PLC), only the inverter connected to the same phase will receive it, thus ensuring the right grouping of the inverters. However, if the distress signal is sent using another technology (e.g. GPRS), the phase of each inverter must first be identified, for example using voltage correlation [11].

IV. Comparison control schemes

The performance of the distributed algorithm is compared to those of two other algorithms. The first one is fully distributed and does not require a model of the network. It is the on-off algorithm already implemented in PV units. The second one is a more elaborate, centralized control scheme based on an optimal power flow and a detailed model of the network.

A. On-off control algorithm

According to EN 50160, the inverters must disconnect if the ten-minute moving average of the voltage at their connection point is higher than 1.1 p.u. Moreover, they must disconnect immediately if the instantaneous voltage is higher than 1.15 p.u.

1) Controller modes: The on-off control algorithm has two modes: an MPPT mode where the active power production is maximised, and an off mode, where the production is shut down. If there are no overvoltages, the PV units are in MPPT mode. If the voltage at their connection point is higher than 1.1 p.u., they switch to the off mode. Let $\mathcal{G}^{(V_{\max})}$ be the subset of PV units observing an overvoltage for the time step $t-1$.

$$P_{set,t}^{(i)} = 0, \forall i \in \mathcal{G}^{(V_{\max})} \tag{11}$$

The production of active power stays at zero for one minute and the PV units then switch back to the MPPT mode. If an overvoltage occurs anew, they switch back to the off mode.

With this algorithm, the production or absorption of reactive power is always equal to zero.

$$Q_{set,t}^{(i)} = 0, \ \forall i \in \mathcal{G} \tag{12}$$

2) Practical implementation: This algorithm is the one currently implemented in commercial inverters. It only relies on local measurements and controls. The inverters constantly monitor the voltage at their terminal and if an overvoltage occurs, they shut down the production.

B. Unbalanced Optimal Power Flow Control Algorithm

A centralised solution to optimize the active and reactive power production of the inverters can take the form of a three-phase Optimal Power Flow (OPF) (See [12] for more information on unbalanced OPF).

1) Optimisation variables: Strictly speaking, optimisation variables are the active and reactive power produced by the PV units: $P_t^{(g)}$ and $Q_t^{(g)}$, $\forall g \in \mathcal{G}$. However, the voltages, currents and line losses are included in the optimisation variables, since they are not explicitly linked to the injected powers. This simplifies the definition of the constraints, e.g. the voltage constraints. The optimisation variables are thus:

$$P_t^{(g)}, Q_t^{(g)}, \quad \forall g \in \mathcal{G} \tag{13}$$

$$I_t^{(i,c)}, \quad \forall i \in \mathcal{G} \cup \mathcal{B} \cup \mathcal{L}, c \in \mathcal{C} \tag{14}$$

$$L_t^{(b,c)}, \quad \forall b \in \mathcal{B}, c \in \mathcal{C} \tag{15}$$

$$V_t^{(n,c)}, \quad \forall n \in \mathcal{N}, c \in \mathcal{C} \tag{16}$$

2) Constraints: All the equations and inequalities presented in Section II are included as constraints of the OPF.

3) Optimisation criterion: The optimisation criterion can be defined as:

$$\max \sum_{g \in \mathcal{G}} P_t^{(g)} - \sum_{b \in \mathcal{B}} \sum_{c \in \mathcal{C}} L_t^{(b,c)} \tag{17}$$

With that formulation, the flow of active power exported by the LV network through the LV/MV transformer is maximised. On a physical point of view, applying the solution of this optimisation problem to the inverters ensures two desirable behaviours: (i) the increase in PV production will not be at the expense of an increase in network losses to a point where the increment in the losses is larger than the increment in the PV power; (ii) if the maximum limit of PV production is reached and some operational margins in reactive power remain, the optimisation will minimise the losses.

4) Practical implementation: A centralised control scheme comprises three different parts. The first one is composed of the infrastructure necessary to evaluate the state of the system it controls. The second part is the controller itself. It computes the control actions from the (previous) information. The third and last part is the infrastructure used for sending and applying its control actions. A centralised scheme based on an OPF would require a detailed model of the network that must be kept up-to-date, and an extended communication infrastructure.

V. Numerical simulations

This section presents the methods used to solve the power flow and the optimal power flow. It also describes the input of the simulations, i.e. the test network, the loads, the different scenarios, as well as the various numerical values chosen for the parameters.

A. Power flow

In the case of LV networks, two methods are commonly used to solve the power flow equations: (i) the Newton-Raphson method applied to the power flow equations expressed in terms of current injections [13], [14], [15], and (ii) the Backward Forward Sweep algorithm [16], [9]. Given its simple implementation and the radial nature of LV networks, we have chosen the latter and implemented it in Python.

B. Time sequence of actions

The simulations have a time step of one minute. They are first initialized with a power flow. Then, for each time step, the sequence of actions is as follows: (i) Based on the voltages from the previous time step, all controllers compute and apply their control actions, i.e. they specify the active and reactive power set points of the PV unit they control. (ii) A power flow is solved taking into consideration the current energy consumption and production. The process is repeated until the end of the simulations.

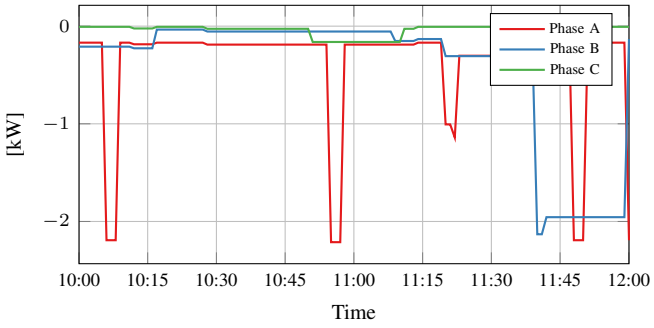

Fig. 3: Active power consumption of L_{18}.

C. Three-phase OPF

The optimisation model is created with Pyomo and solved using the interior point method with IPOPT. The optimisation problem is expressed in rectangular coordinates, i.e. the complex variables and equations are separated into their real and imaginary parts. The initial feasible solution is coming from power flow calculation assuming that the PV production is zero. Since the power flow equations and some constraints are non-linear, there is no guarantee of reaching a global optimum.

D. Test network

The test network used for this study is a single feeder from an existing Belgian LV distribution network with a star configuration 400V/230V and an ungrounded neutral. Detailed unbalanced three-phase four-wire modelling of the network has been used according to [9] based on the data provided by the Distribution System Operator (DSO) (topology, line length, cable type, etc.). Figure 5 shows a graphical representation of the test network. The overhead lines are BAXB cables (Aluminium 3x70 mm^2 1x54 mm^2), and the connexion to the house uses BXB cables (Aluminium 4x10 mm^2). The impedance matrices $Z^{(b)}$, $\forall b \in \mathcal{B}$ are computed with PowerFactory.

E. PV connection scenarios

As can be seen in Figure 5, each house is equipped with a PV unit. There are 17 5 kWp single-phase PV units, and two three-phase units of 7 kWp each (PV_9 and PV_{14}). They will be used to exhibit the behaviour of the three-phase group of inverters. According to the German and Italian standard, all PV units have a minimum power factor $PF_{\min}$ of 0.95.

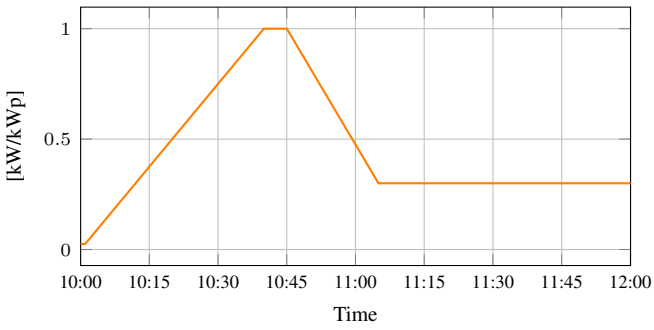

Fig. 4: Maximum power point for the PV units in kW/kWp.

Different scenarios for the connection of the single-phase PV units are studied. In all of them, the peak power of the PV unit is unchanged, only their connection to the three phases changes. The two three-phase units remain unchanged throughout each scenario.

- *3P*: The single-phase units are converted to three-phase ones. The production is thus balanced.
- *ABC*: PV_0 is connected to Phase A, PV_1 to Phase B, PV_2 to Phase C. This pattern is repeated until the end of the feeder.
- *AABC*: PV_0 is connected to Phase A, PV_1 to Phase A, PV_2 to Phase B, PV_3 to Phase C. This pattern is repeated until the end of the feeder.
- *AAABC*: PV_0 is connected to Phase A, PV_1 to Phase A, PV_2 to Phase A, PV_3 to Phase B, PV_3 to Phase C. This pattern is repeated until the end of the feeder.
- *AAA*: All single-phase inverters are connected to Phase A.

F. Loads

The consumption of the loads is defined by profiles created using a three-phase unbalanced version of [17]. The example of the active power consumed by load L_{18} is presented in Figure 3. The loads are assumed to have a constant power factor of 0.95 lagging.

G. Numerical values of the parameters

The voltage should lie within $\pm 10\%$ of the nominal voltage, hence $V_{\min}$ = 0.9 p.u. and $V_{\max} = 1.1$ p.u. The different values for the timers of the distributed control scheme are $t_{DQ} = t_{DP} = 5$ min., $t_{reset} = 5$ min., and $t_{RQ} = t_{RP} = 10$ min. In mode $Q_{loc}^{\downarrow\uparrow}(V)$, $V_1 = V_{\min} = 0.9$ p.u., $V_2 = 0.92$ p.u., $V_3 = 1.08$ p.u. and $V_4 = V_{\max} = 1.1$ p.u.

VI. Simulation Results

A. Synthetic production profile

This section demonstrates the behaviour of the distributed algorithm in the case of a synthetic production profile (Figure 4), specially designed to bring to light the different modes of the distributed control algorithm. The connection scenario used for the PV units is *AABC* to have a reasonably unbalanced network.

1) Phase B Group: Figure 6 shows the phase-to-neutral voltage of the single-phase PV unit PV_{11}, the one connected to Phase B which exhibits the highest voltage. As can be seen, there are no voltage problems for Phase B. Thus, no reactive power is absorbed by PV units belonging to the Phase B group, nor is active power curtailed.

2) Phase C Group: Figure 7 displays the actions of the controllers for the Phase C, Phase A and three-phase groups. Present n this figure are the PV units of each group which recorded the highest voltages at their point of connection, i.e. PV_{12} (Phase C), PV_{13} (Phase A) and PV_{14} (three-phase). The first line of graph shows the phase-to-neutral voltages, the second one the mode in which the controllers are, the

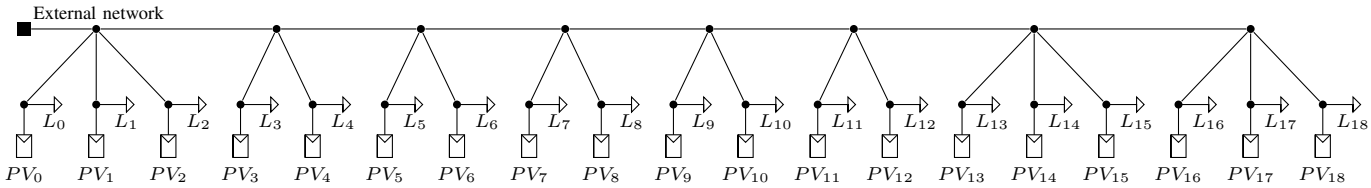

Fig. 5: Graphical representation of the test network.

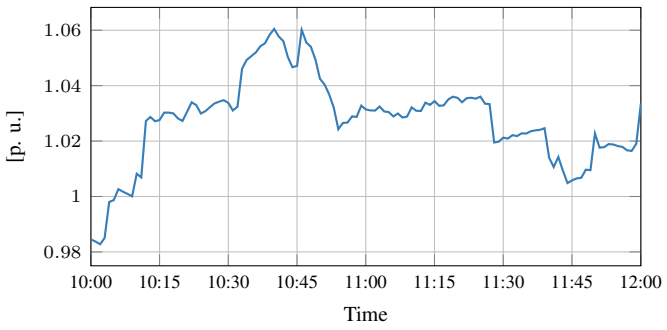

Fig. 6: Phase-to-neutral voltage for PV_{11} (connected to Phase B).

third one corresponds to the active power produced, and the final one corresponds to the reactive power absorption.

Focusing on the first column of Figure 7, one can see that the voltage is close to 1.1 p.u., the overvoltage limit. The voltage exceeds this limit two times: one time at 10:41 and the other one at 10:46. At those moments, the PV units send a distress signal to all PV units connected to phase C, including the three-phase ones, and they switch to mode $Q^{\downarrow}$, where they gradually absorb more reactive power. Once the overvoltage has cleared, the PV units first move to Mode $Q^{\rightarrow}$, where they wait until they can attain Mode $Q^{\uparrow}$, where they decrease the absorption of reactive power. Finally, since there is no new overvoltage, they proceed to Mode $Q_{loc}^{\downarrow\uparrow}(V)$, the normal mode of operation.

The PV units of the Phase C group never resort to active power curtailment, and only use reactive power to mitigate the voltage problems.

3) Phase A Group: The voltage of Phase A is the highest of the three phases. This is related to the fact that the majority of PV units are connected to it. Two overvoltages occur from 10:24 to 10:32, and from 10:44 to 10:45. During the first one, the PV units move to Mode $Q^{\downarrow}$, where they increase their absorption of reactive power. Unfortunately, the use of reactive power to lower the voltage is not sufficiently effective to mitigate the overvoltage, and after t_{DQ} minutes (5 min), they switch to the active power curtailment mode (Mode $P^{\downarrow}$). The latter has two effects on the inverters: the first one is the curtailment of active power, and the second one is the induced reduction of the maximum amount of reactive power that they can absorb owing to their capability curve. At 10:32, when the overvoltage is solved, the inverters move to waiting Mode $P^{\rightarrow}$, where they keep the active power constant for t_{reset} minutes, until they try to increase the active power, resulting in another overvoltage, forcing them to return to Mode $P^{\downarrow}$. The second time the inverters increase the active power, the maximum power point limit is sufficiently low for them to reach the limit without generating an overvoltage. They then proceed to Mode $Q^{\downarrow}$, where they gradually limit the absorption of reactive power to reach the value dictated by Mode $Q_{loc}^{\downarrow\uparrow}(V)$. Finally, reactive power absorption spikes at 11:42 due to the sudden increase in the voltage, a behaviour generated by the $Q_f(V)$ curve of Mode $Q_{loc}^{\downarrow\uparrow}(V)$.

4) Three-phase group: The three-phase group is the most impacted by the voltages given that it records the overvoltages in the three phases. Indeed, its actions are dictated by the union of the distress signals in all the phases. The main difference between the Phase A group and the three-phase group is the increased curtailment from 10:45 to 10:49 due to the overvoltage in Phase C, that is not yet relieved, forcing the three-phase inverters to proceed to additional curtailment.

5) External network: Figure 8 shows the power flowing in the line at the beginning of the feeder. First, there is no PV production and the feeder imports power from the external network. At 10:00, 10:07, 10:10, reverse power flows occur respectively in Phase C, A and B, which will last for the length of the simulations. The graph shows that power can flow in opposite directions at the same time. It also clearly shows that Phase A hosts the most PV production, and one can observe the two spikes around 10:30 and 10:45 due to active power curtailment.

B. Comparison between algorithms

The three algorithms are compared in the setting of a sunny day where the maximum PV power ($P_{MPP,t}$) follows the profile shown in Figure 9. The maximum power is scaled according the peak power of the PV unit.

1) Curtailed energy: Figure 10 shows the total energy curtailed during the simulation. For each scenario, the relative performance of the algorithms is the same, with the OPF outperforming the distributed algorithm and the on-off algorithm. This is to be expected since the OPF performs an optimisation over the entire system with a detailed model of this one. The gap of performance between the three algorithms reduces when Phase A is increasingly loaded.

Of course, the curtailed energy increases when more PV units are connected to the same phase as imbalance reduces the hosting capacity of the network [18]. Indeed, the voltage

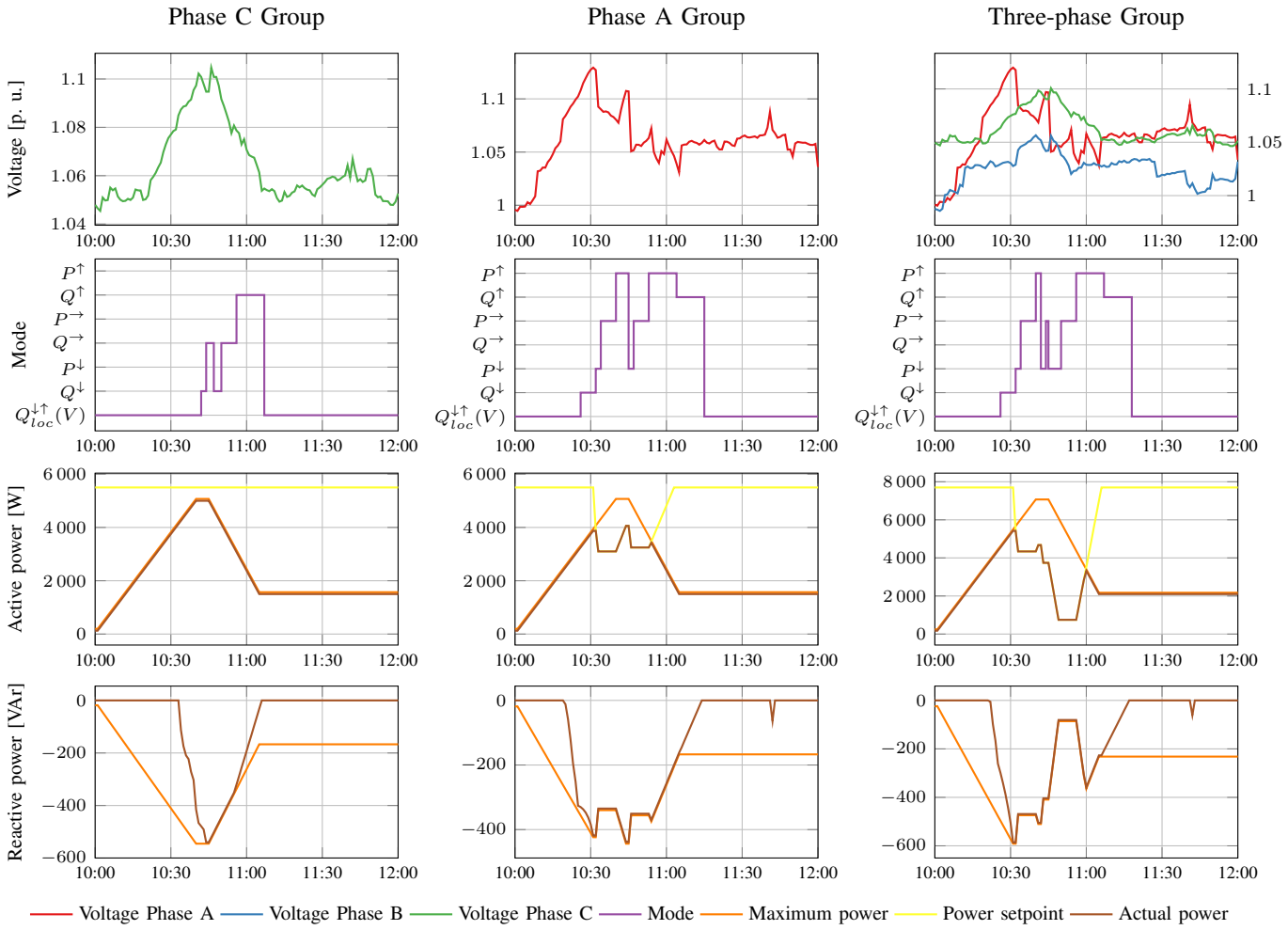

Fig. 7: Active and reactive power production and absorption, controller mode and phase-to-neutral voltage of PV_{12} (Phase C group), PV_{13} (Phase A group) and PV_{14} (three-phase group).

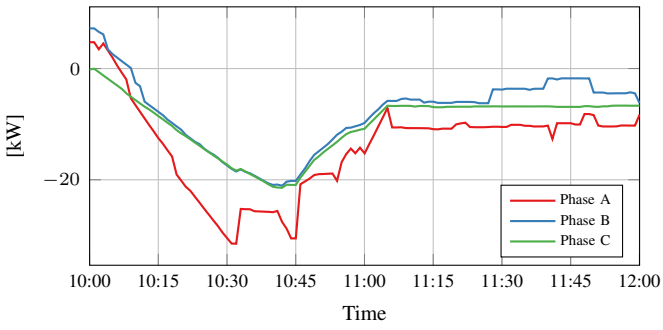

Fig. 8: Distribution transformer: active power in each phase.

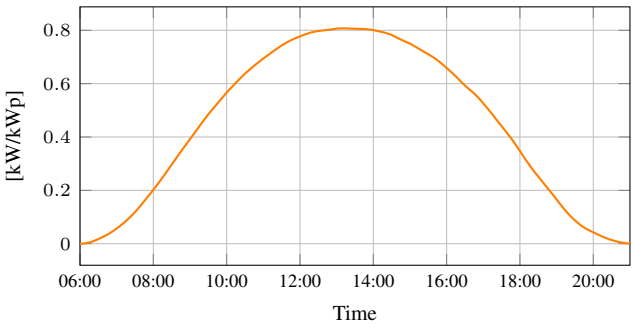

Fig. 9: Maximum power for the PV units of 5 kWp

rise in one phase depends on the amount of power transferred by the conductor.

Finally, the distributed algorithm and the OPF have poorer performances in scenario *3P* than in scenario *ABC*, because single-phase inverters are better suited to minimize curtailment, when the consumption of the houses is not balanced. Given that they can operate independently of the other phases,

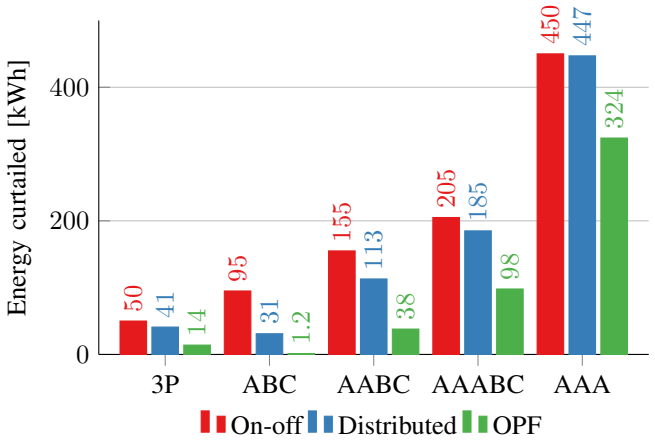

Fig. 10: Curtailed energy

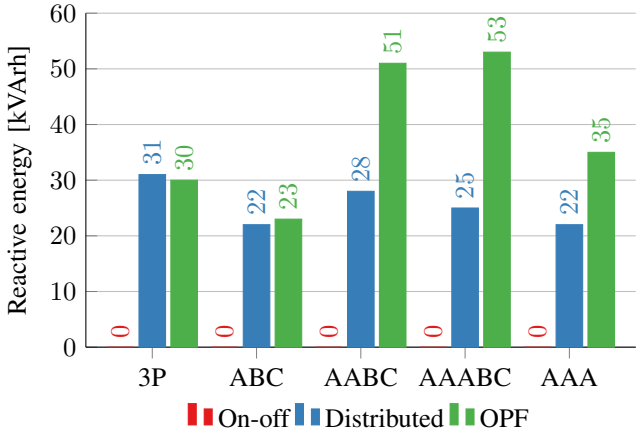

Fig. 11: Reactive energy

single-phase inverters only curtail power in the phase(s) with a voltage problem, whereas three-phase inverters curtail power in the three phases, even if only one of them suffers from an overvoltage.

2) Reactive power usage: Figure 11 shows the use of reactive energy during the simulations. It is expressed in kVArh and counted regardless of its sign (absorption or production). Of course, the on-off algorithm makes no use of reactive power

The available reactive power is strongly dependent on the active power production, and thus the curtailed power, as it reduces the maximum amount of reactive power than the PV unit can produce or absorb (cf. Section II-C2). This explains the smaller use of reactive energy in the last configuration, as it is the configuration where power is most curtailed.

The distributed algorithm uses reactive power in a constant manner regardless of the scenario. Indeed, given that the maximum power that one phase can accommodate should remain almost identical between the scenarios, the reactive power energy use is relatively constant. However, the OPF produces and absorbs more reactive power because it optimises the three phases at the same time, leading to the production of reactive power in some phases to produce more active power in the others, whereas with the distributed algorithm, reactive power is used independently of the other phases.

3) Losses: The losses for the OPF are almost always larger than for the other algorithms. It increases the losses in the network to allow the production of more photovoltaic energy. This is linked to the two previous figures. However, the objective of the OPF ensures that the losses are not increased to a point where they would become prohibitive in regards to the marginal produced energy.

Moreover, the losses decrease from scenario *ABC* to scenario *AAA* because of the increased curtailed energy which lowers the currents in the network.

The losses with the on-off algorithm – especially in configuration *AAA* – are relatively high compared to the ones with the distributed algorithm that uses reactive power as a support. One explanation is the higher variations of current with the on-off algorithm. With the rapid disconnection and reconnection of the PV units, large temporary currents occur in the network. Since the losses are proportional to the square of the currents, if the variations of currents are higher, even if they have the same mean value, the losses will be larger. Furthermore, the rapid variations of current lead to voltage flicker, as shown in Figure 13, an effect undesirable for the proper network operations.

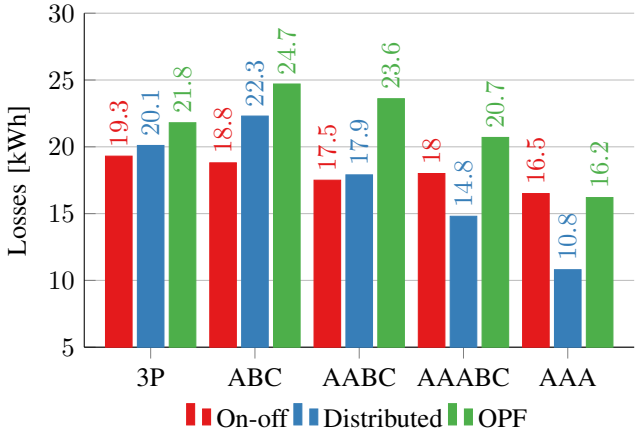

Fig. 12: Losses

VII. Conclusion

In this paper, we have presented the extension of a distributed control scheme, which controls the active and reactive power production of PV units, to prevent overvoltages. It does not require a detailed model of the LV network, and it only relies on limited communication in the form a distress signal when there is an overvoltage, in order to pool the resources.

The control scheme works by first partitioning the inverters into four groups, three for the single-phase inverters (one for each phase), and one for the three-phase ones. Each group then applies independently a distributed algorithm similar to the one presented in [1]. The single distress signal of [1] is

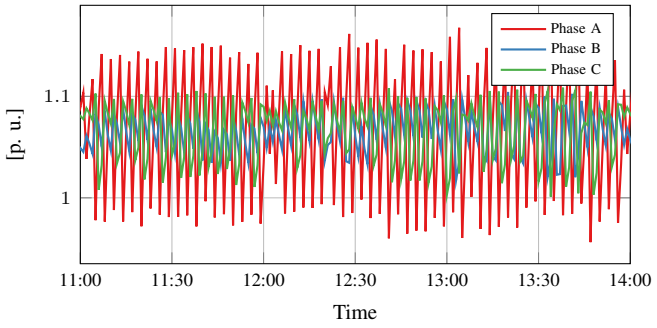

Fig. 13: NDum15: Phase-to-neutral voltage (on-off – *AABC*). The voltage flicker is due to the rapid connection and disconnection of the PV units.

replaced by three distress signals, one for each phase. Since a group only reacts to the distress signal of the phase to which it is associated, single-phase inverters do not curtail power in a phase without voltage problems.

The behaviour of the proposed scheme is first illustrated and explained. Its performance are then compared to those of two reference schemes, one based on the on-off algorithm and the other one based on an unbalanced OPF. Its resulting total curtailed energy always lies between the two, with the on-off algorithm presenting the poorest performance, and the proposed algorithm losing its edge when the network is strongly unbalanced. It performs indeed better when the connection of the single-phase PV units is balanced between the phases. Finally, it generates less losses in the network than the other schemes, but at the expense of the produced energy, compared to the OPF.

Future works could include the detailed analysis of the reactive power produced by the OPF. Indeed, the use of reactive power in the phases that do not have overvoltage problem is changed to allow more PV energy to be produced in the problematic phases. This needs to be further studied to replicate this behaviour in a distributed way.

References

[1] F. Olivier, P. Aristidou, D. Ernst, and T. Van Cutsem, "Active management of low-voltage networks for mitigating overvoltages due to photovoltaic units," *IEEE Transactions on Smart Grid*, vol. 7, no. 2, pp. 926–936, mar 2016.

[6] W. H. Kersting, *Distribution System Modeling and Analysis*. Boca Raton: CRC Press, 2006.

[2] X. Su, M. A. Masoum, and P. Wolfs, "Comprehensive optimal photovoltaic inverter control strategy in unbalanced three-phase four-wire low voltage distribution networks," *IET Generation, Transmission & Distribution*, vol. 8, no. 11, pp. 1848–1859, nov 2014.

[3] X. Su, M. A. S. Masoum, and P. J. Wolfs, "Optimal PV inverter reactive power control and real power curtailment to improve performance of unbalanced four-wire LV distribution networks," *IEEE Transactions on Sustainable Energy*, vol. 5, no. 3, pp. 967–977, jul 2014.

[4] E. Dall'Anese, G. B. Giannakis, and B. F. Wollenberg, "Optimization of unbalanced power distribution networks via semidefinite relaxation," in *Proc. of the 2012 North American Power Symposium (NAPS)*, 2012.

[5] K. H. Chua, Y. S. Lim, P. Taylor, S. Morris, and J. Wong, "Energy storage system for mitigating voltage unbalance on low-voltage networks with photovoltaic systems," *IEEE Transactions on Power Delivery*, vol. 27, no. 4, pp. 1783–1790, oct 2012.

[7] A. J. Urquhart, "Accuracy of low voltage distribution network modelling," Ph.D. dissertation, Loughborough University, 2016.

[8] D. Das, H. Nagi, and D. Kothari, "Novel method for solving radial distribution networks," *IEE Proceedings - Generation, Transmission and Distribution*, vol. 141, no. 4, p. 291, jul 1994.

[9] R. Ciric, A. Feltrin, and L. Ochoa, "Power flow in four-wire distribution networks-general approach," *IEEE Transactions on Power Systems*, vol. 18, no. 4, pp. 1283–1290, nov 2003.

[10] K. M. Sunderland and M. F. Conlon, "4-Wire load flow analysis of a representative urban network incoprating SSEG," in *Proc. of 2012 47th International Universities Power Engineering Conference (UPEC)*, 2012.

[11] F. Olivier, A. Sutera, P. Geurts, R. Fonteneau, and D. Ernst, "Phase identification of smart meters by clustering voltage measurements," in *Proc. of XXth Power System Computation Conference (PSCC)*, Dublin, 2018.

[12] S. Bruno, S. Lamonaca, G. Rotondo, U. Stecchi, and M. La Scala, "Unbalanced three-phase optimal power flow for smart grids," *IEEE Transactions on Industrial Electronics*, vol. 58, no. 10, pp. 4504–4513, oct 2011.

[13] P. Garcia, J. Pereira, S. Carneiro, V. da Costa, and N. Martins, "Three-phase power flow calculations using the current injection method," *IEEE Transactions on Power Systems*, vol. 15, no. 2, pp. 508–514, may 2000.

[14] M. J. Alam, K. M. Muttaqi, and D. Sutanto, "A three-phase power flow approach for integrated 3-wire MV and 4-wire multigrounded LV networks with rooftop solar PV," *IEEE Transactions on Power Systems*, vol. 28, no. 2, pp. 1728–1737, 2013.

[15] D. Penido, L. Araujo, J. Pereira, P. Garcia, and S. Carneiro, "Four wire newton-rapshon power flow based on the current injection method," in *Proc. of IEEE PES Power Systems Conference and Exposition*, New York, 2004.

[16] C. Cheng and D. Shirmohammadi, "A three-phase power flow method for real-time distribution system analysis," *IEEE Transactions on Power Systems*, vol. 10, no. 2, pp. 671–679, may 1995.

[17] I. Richardson, M. Thomson, D. Infield, and C. Clifford, "Domestic electricity use: a high-resolution energy demand model," *Energy and Buildings*, vol. 42, no. 10, pp. 1878–1887, oct 2010.

[18] B. Bletterie, A. Goršek, A. Abart, and M. Heidl, "Understanding the effects of unsymmetrical infeed on the voltage rise for the design of suitable voltage control algorithms with PV," in *Proc. of the 26th European Photovoltaic Solar Energy Conference and Exhibition (EU PVSEC)*, Hamburg, 2011.